Ann. Geophysicae 18, 1172–1181 (2000) © EGS – Springer-Verlag 2000

Annales Geophysicae

Auroral *E*-region electron density gradients measured with EISCAT

C. Haldoupis[1], **K. Schlegel**[2], **G. Hussey**[3]

[1] Physics Department, University of Crete, Iraklion, Greece
[2] Max-Planck Institut für Aeromonie, Katlenburg-Lindau, Germany
[3] Department of Physics and Engineering Physics, University of Saskatchewan, Canada

Received: 24 January 2000 / Revised: 7 April 2000 / Accepted: 12 April 2000

Abstract. In the theory of *E*-region plasma instabilities, the ambient electric field and electron density gradient are both included in the same dispersion relation as the key parameters that provide the energy for the generation and growth of electrostatic plasma waves. While there exist numerous measurements of ionospheric electric fields, there are very few measurements and limited knowledge about the ambient electron density gradients, ∇N_e, in the *E*-region plasma. In this work, we took advantage of the EISCAT CP1 data base and studied statistically the vertical electron density gradient length, $L_z = N_e/(\mathrm{d}N_e/\mathrm{d}z)$, at auroral *E*-region heights during both eastward and westward electrojet conditions and different ambient electric field levels. Overall, the prevailing electron density gradients, with L_z ranging from 4 to 7 km, are found to be located below 100 km, but to move steadily up in altitude as the electric field level increases. The steepest density gradients, with L_z possibly less than 3 km, occur near 110 km mostly in the eastward electrojet during times of strong electric fields. The results and their implications are examined and discussed in the frame of the linear gradient drift instability theory. Finally, it would be interesting to test the implications of the present results with a vertical radar interferometer.

Key words: Ionosphere (auroral ionosphere; ionospheric irregularities; plasma waves and instabilities)

1 Introduction

Our basic understanding of the unstable *E*-region ionosphere relies on the theory of the "modified two stream" and "gradient drift" plasma instabilities, e.g., see the classic review by Fejer and Kelley (1980). As shown in many papers, the effects of both instability mechanisms are combined in the same dispersion relation of the linear fluid theory, which derives from the electron and ion equations of motion and equations of continuity. For the usual case of plasma waves propagating perpendicular to the magnetic field, the solution of the dispersion equation, for wavelengths $\lambda = 2\pi/k$ ranging from a few meters to maybe a few hundred meters, takes the familiar form (e.g., see Fejer *et al.*, 1984)

$$\omega_k = \frac{\mathbf{k}\cdot\mathbf{V_d}}{(1+\psi)} \tag{1}$$

$$\gamma_k = \frac{\psi}{(1+\psi)}\left(\frac{\omega_k^2 - k^2C_s^2}{\nu_i} + \frac{\Omega_e\omega_k}{\nu_e k L_\perp}\right) - 2\alpha N_e \ , \tag{2}$$

where all symbols have their usual meaning, that is, ω_k is the wave angular frequency, γ_k is the growth rate, ν and Ω are the collision and gyro frequencies, $\psi = (\nu_e\nu_i)/(\Omega_e\Omega_i)$, C_s is the ion acoustic speed, N_e is the mean electron density and α is the recombination coefficient. Furthermore, $\mathbf{V_d}$ is the relative electron-ion drift velocity which is taken to be approximately equal to the electron Hall drift $\mathbf{E}\times\mathbf{B}/B^2$, and $L_\perp = N_e/(\mathrm{d}N_e/\mathrm{d}x)$ is the electron density gradient length perpendicular to $\mathbf{B}$ and parallel to $\mathbf{E}$, taken as positive if $(\nabla N_e)_\perp \cdot \mathbf{E} > 0$.

As seen from these equations, an ambient electric field $\mathbf{E}$ and an electron density gradient ∇N_e constitute the agents that provide the free energy for destabilization of the *E*-region plasma. Knowledge of them is therefore of importance to theoretical calculations and simulation studies as well as in the interpretation of observations. With respect to $\mathbf{E}$, there exist many direct and indirect measurements of *E*-region electric fields, mostly made with incoherent scatter radars, like EISCAT, which measure *F*-region $\mathbf{E}\times\mathbf{B}$ ion drifts on a routine basis (e.g., see Kelley, 1989). On the other hand, our knowledge is limited about the prevailing electron

Correspondence to: K. Schlegel
e-mail: schlegel@linmpi.mpg.de

density gradients at *E*-region heights where conditions for instability are optimal. We believe there is a need for *E*-region electron density gradient estimates to be better known and quantified, and this work aims to serve this purpose.

In the present study, we exploit the large EISCAT Common Program 1 (CP1) data base to measure the dominant vertical electron density gradient lengths $L_z = N_e/(\mathrm{d}N_e/\mathrm{d}z)$ at auroral *E*-region heights during both eastward and westward electrojet conditions and for different electric field levels. In addition we consider and discuss the consequences of our findings by applying the dispersion relation of the gradient drift instability.

2 Auroral *E*-region vertical density gradients

The present study deals only with vertical ionization gradients, $(\nabla N_e)_z$, which relate to *E*-region electron density profiles that peak mostly between about 100 and 110 km. The variations in the profiles are controlled by ionization production and loss mechanisms relating to direct solar ultraviolet radiation and/or energetic particle precipitation during magnetically disturbed conditions. Photoionization-produced vertical gradients are more intense at lower latitudes, particularly at the equator where they are known to play a key role in destabilizing the equatorial electrojet plasma through the gradient drift instability (Fejer *et al.*, 1975; Pfaff *et al.*, 1987). Also, strong vertical gradients can exist at midlatitude during sporadic *E*-layer conditions. These are linked directly to the occurrence of midlatitude coherent backscatter from plasma irregularities excited primarily by the gradient drift instability (e.g., see Riggin *et al.*, 1986; Haldoupis and Schlegel, 1993; Bourdillon *et al.*, 1995, among others).

Since the scale length $L_\perp$ in Eq. (2) relates to the density gradient component perpendicular to **B**, the destabilizing role of a vertical density gradient is much less severe in the auroral zone because of the larger magnetic dip angles, as compared to at lower latitudes. Nevertheless, the effect of $(\nabla N_e)_z$ in the instability process cannot be ignored in the aurora, especially during magnetically active conditions. This claim is supported from in situ rocket observations (Pfaff *et al.*, 1984; Pfaff, 1986; Kelley, 1989) which suggest that, in addition to the electric field, the vertical density gradient $(\nabla N_e)_z$ does also affect the level of electrostatic turbulence in the auroral electrojets.

Before presenting the method of analysis and the observations, we refer briefly to the vertical density gradient role in the auroral instability process. This topic was first taken up by Greenwald (1974). The situation is summarized in Fig. 1 where typical N_e profiles are depicted in the meridian plane during both the eastward and westward electrojet. In interpreting this figure, one should keep in mind that the gradient drift term in Eq. (2) alters the two stream instability threshold, as discussed by Farley and Fejer (1975). A destabilizing density gradient having a component

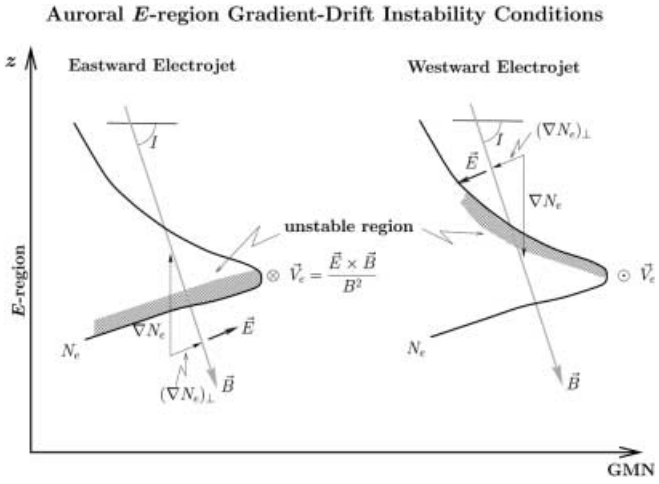

Fig. 1. Gradient drift instability conditions and related geometry in the magnetic meridian plane for a typical electron density profile in the auroral eastward and westward electrojet plasma

parallel to **E**, lowers the two stream instability threshold below C_s and increases the linear growth rate. The opposite is true for a stabilizing gradient component anti-parallel to the ambient electric field. In addition, and because the gradient drift term in Eq. (2) is inversely proportional to k, these effects are much more favorable for longer than for shorter wavelength waves.

Figure 1 sketches the picture expected in the horizontally stratified auroral *E*-region, with $\hat{x}$ pointing to geomagnetic north and $\hat{z}$ to the zenith. Since the magnetic field forms a dip angle I, the density gradient component that enters in the dispersion relation is $(\nabla N_e)_\perp = (\nabla N_e)_z \cos I$. In this way, the destabilizing effects of the vertical gradients are confined at the bottom (top) of the N_e profile during eastjet (westjet), whereas the unstable gradient-drift waves propagate westward (eastward), along $\mathbf{E}\times\mathbf{B}$. On the other hand, a vertical density gradient becomes stabilizing at the top and bottom of the profiles for the eastjet and westjet, respectively.

One might notice that in the geometry of Fig. 1, the inclined magnetic field couples the unstable side at the top or bottom of the electron density profile with the stable bottomside or topside, respectively. This can counteract the instability because perturbation electric fields which develop in the unstable side can map along magnetic field lines and possibly be shorted out at the stable side. Because these non-local effects have not yet been studied theoretically we cannot assess their importance for the present study, therefore no additional consideration is given in the rest of the work.

Finally, horizontal, or lateral, electron density gradients must also be present in the auroral plasma. For example, the auroral ionosphere itself is horizontally inhomogeneous since it is aligned in the east-west direction, having well-defined equatorward and poleward ionization boundaries. In addition, the auroral activity is often dominated by intense auroral arcs with very sharp edges where horizontal electron density gradients are likely to be very large and thus have

significant effects in the instability process, as discussed for example by St.-Maurice *et al.* (1994) and Haldoupis *et al.* (1995). These horizontal gradients cannot be measured by the EISCAT CP1 mode, and therefore were not dealt with in the present study.

3 Data and method of analysis

In the present analysis, we used a large number of EISCAT CP1-K observations. In the CP1 mode, EISCAT is run continuously for a 24-h period and measures ionospheric profiles of electron density, electron and ion temperatures and velocity along the radar beam as a function of altitude, for altitudes between 90 and 180 km. The radar points at an elevation angle of 76.5° to the south, approximately along the local magnetic field line at the EISCAT site near Tromsø. In addition, incoherent tristatic Doppler measurements are also performed at a fixed *F*-region altitude on the same magnetic field line, from which the cross-field ion drift velocity, or alternatively the convection **E** field and subsequently the *E*-region $\mathbf{E} \times \mathbf{B}$ electron drift, is estimated. The integration time used in the CP1-K mode is 2 min and the altitude resolution at *E* region altitudes is close to 3 km. The electron densities used in the analysis are corrected to account for unequal temperatures and Debye-length effects (e.g., see Schlegel, 1988). In general, the uncertainties in the incoherent scatter measurements are expected to be between 5 to 10%, depending on SNR. In the analysis we have considered only those profiles for which the signal-to-noise ratio was reasonably high (SNR > 0.02).

The CP1 measurements used in the analysis are from a total of 25 days of EISCAT operation, from 1993, 1995, 1996 and 1998. Figure 2 includes a table, showing the number of CP1 days per year, and a histogram showing how these days are distributed with respect to the mean level of geomagnetic activity expressed by the daily ΣK_p index. As seen, most of the days used represent moderately disturbed conditions with ΣK_p ranging between about 10 and 30, whereas there are a few days when $\Sigma K_p > 35$ and one day when conditions were strongly disturbed with ΣK_p nearing 50.

With respect to the prevailing electron drifts, or electric fields, the situation is summarized, for the entire data set, in Fig. 3. This is a scatter plot showing how the *E*-region electron drift magnitude is distributed relative to the drift direction. As seen, the points are divided evenly in two groups: one relates to predominantly eastward electron drift directions clustered about 90° and corresponding to westward electrojet conditions which dominate the post-midnight sector, whereas the other subset of points has predominantly westward electron drifts about 270° which are known to occur in the afternoon/pre-midnight local time sector during eastward auroral electrojet occurrences. Also, the great majority of points have drift magnitudes less than 800 m/s, that is, electric fields less than about 40 mV/m. On the other hand, there are a great deal of points with drifts higher than 800 to 1000 m/s relating to strong

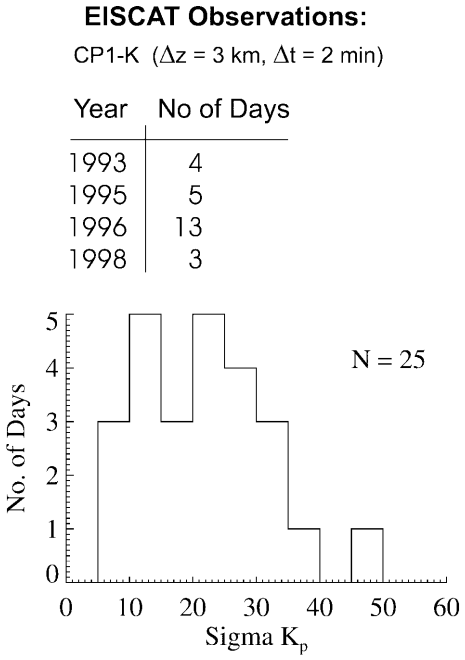

Fig. 2. Days of EISCAT CP1-K measurements used in the analysis and the corresponding distribution with respect to the mean geomagnetic activity level

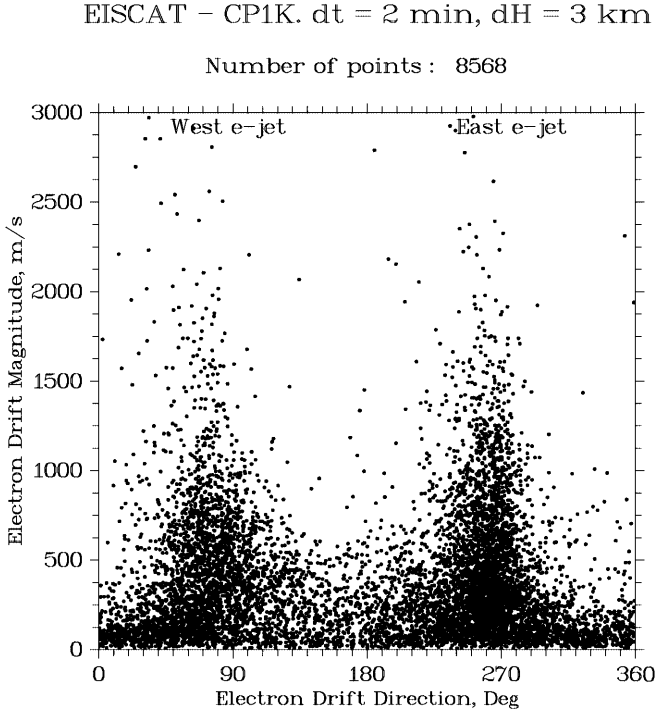

Fig. 3. Scatter plot of *E*-region ($\mathbf{E} \times \mathbf{B}$) electron drift magnitude versus electron drift direction measured by EISCAT for the entire data set analyzed (8568 profiles). The measurements are equally representative of both eastward and westward auroral electrojets. Note that a 100 m/s electron drift corresponds approximately to 5 mV/m electric field; the electric field points 90° clockwise the electron drift direction

electric field occurrences which are known to be accompanied by significant *E*-region electron gas heating (e.g., see Schlegel and St.-Maurice, 1981; St.-Maurice *et al.*, 1990).

In the analysis, we consider only electron density profiles in the *E*-region altitude range between 90 and 135 km having their peak usually below 110 km. Basically, it is around the N_e peak that the auroral electrojets maximize and the strongest electrostatic turbulence, caused by the combined action of the two stream and gradient drift plasma instabilities, takes place (e.g., see Pfaff *et al.*, 1984; Kelley, 1989).

To explain the method of analysis we include Fig. 4 showing a typical EISCAT N_e profile between 90 and 135 km with an altitude resolution of $\Delta z \simeq 3$ km. As seen, N_e increases abruptly from $0.5 \times 10^{11}\,\mathrm{m}^{-3}$ at about 95 km to its maximum of $7.8 \times 10^{11}\,\mathrm{m}^{-3}$ near 105 km, and then drops more gradually as we move up in altitude. In this picture, the positive vertical density gradients $\mathrm{d}N_e/\mathrm{d}z$ point upward below 105 km and are steeper than the density gradients above the N_e peak, which are negative pointing downward.

For our purposes, the vertical gradient scale length L_z was computed as follows:

$$L_z = \frac{N_e}{(\nabla N_e)_z} \simeq (z_{i+1} - z_i)\frac{[(N_e)_{i+1} + (N_e)_i]/2}{(N_e)_{i+1} - (N_e)_i} \quad , \qquad (3)$$

and assigned to the altitude $z_i + \Delta z/2$. In this way, the estimated vertical scale lengths L_z for the profile in Fig. 4 are expressed in km and marked by the solid squares in the same plot. As seen, L_z at the lower side of the electron density profile takes positive values near 5 km, whereas at the topside, values are between -15 to -20 km. This procedure was applied to the entire data set which was comprised of more that 8500 electron density profiles.

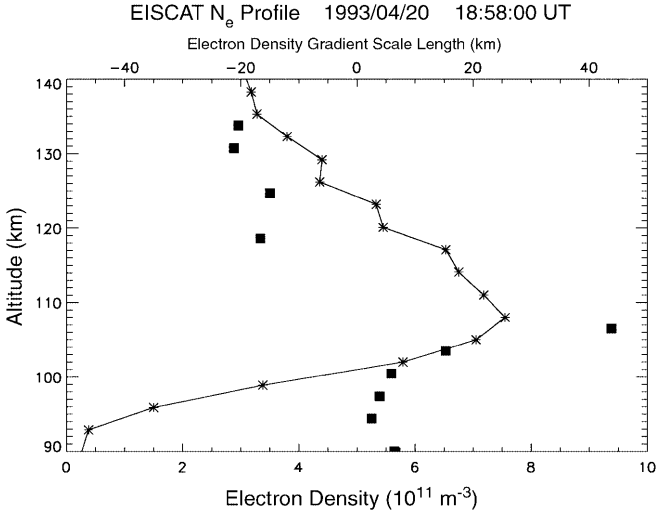

Fig. 4. A typical EISCAT *E*-region electron density profile measured by EISCAT with an altitude resolution near 3 km. The *solid squares* denote the computed vertical plasma density scale lengths, L_z, expressed in km. See text for details

We need to clarify that, although in CP1 mode EISCAT measures the electron density along the magnetic field line near Tromsø, i.e., at about 13.5° off-zenith, these data are used to compute vertical density profiles. This is based on the assumption that the stratified ionosphere is horizontally homogeneous over distances of the order of several km at *E*-region altitudes. Given the large radar integration times used in CP1 mode and the large number of observations considered in the analysis, we believe that, for the purposes of the present statistical study, this assumption is fairly satisfactory.

Finally, we stress that in the nocturnal auroral *E* region, the enhanced electron density profiles observed during magnetically disturbed conditions are mostly determined by the energy spectrum of the precipitating electrons. In addition, these profiles could be affected, but to a much lesser extent, we believe, by vertically induced plasma transport driven by the electric fields, as discussed by Huuskonen *et al.* (1984). Also, it is possible for an auroral density profile to be modified by large-scale instabilities which produce filamentations in electron density aligned preferentially with the magnetic field. The EISCAT CP1 data can be used in a careful analysis, and in conjunction with additional concurrent observations, to possibly differentiate the effects of these causes. This option, however, is certainly beyond the scope of the present study.

4 Results

In this section, the relative distribution of the occurrence of the vertical density gradient scale length, L_z, is presented for *E*-region altitudes between 90 and 135 km. Figure 5 shows in color-coded form the occurrence distribution of scale length L_z normalized to its maximum, for the entire number of CP1 electron density profiles considered in the statistics, that is, 8568 profiles from all 25 days analyzed. The most striking feature is the pronounced peak in relative occurrence at $L_z \simeq 5$ km near 97 km. Another feature is the contrasting difference between the bottomside and topside of the *E*-region electron density peak, that is, below and above 110 km, respectively. The bottomside vertical gradients are, as expected, much steeper, with scale lengths confined inside a well-defined range of values, between about 3 and 15 km. Note that $L_z \sim 3$ km represents the lowest limit of the measurements imposed by the CP1 EISCAT altitude resolution. On the other hand, the topside distribution is rather flat and featureless with scale lengths ranging with equal probability from about -10 km to more than -25 km, regardless of altitude. Finally, the most probable gradient scale length increases with altitude from 95 to 105 km, whereas a secondary peak at about $L_z \simeq 4$ km is also seen near 108 km. The latter, as will be shown, relates to steep electron density profiles peaking higher in the *E*-region during conditions of large electric fields.

The analysis showed systematic changes in the bottomside distribution for different electric field levels.

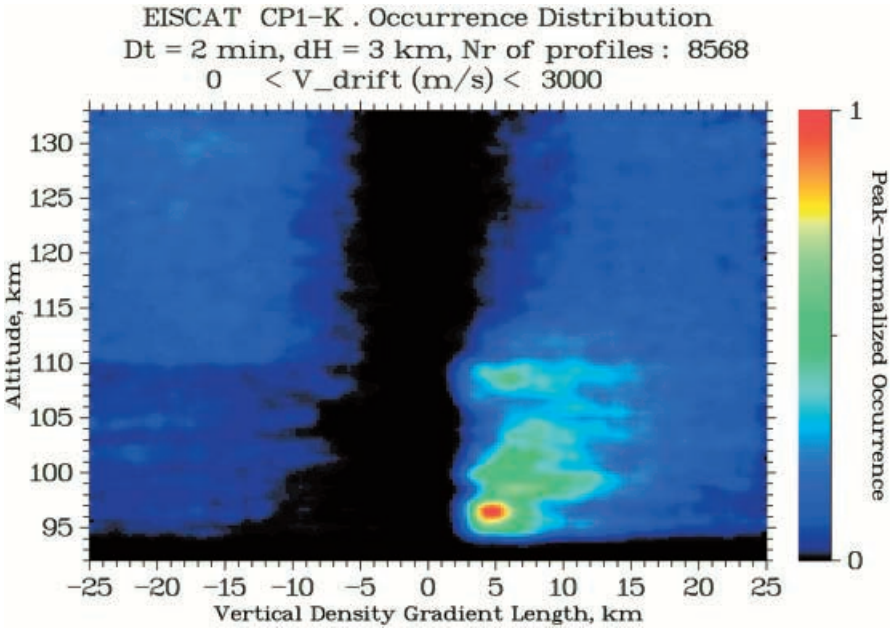

Fig. 5. Normalized distribution of occurrence of the measured vertical electron density scale lengths, $L_z = N_e/(\nabla N_e)_z$, as a function of auroral *E*-region altitude. See text for details

This is illustrated in Fig. 6 which includes three color-coded plots similar to those in Fig. 5. The top plot shows the scale length distribution during low electron drift levels when $\mathbf{E} \times \mathbf{B}/B^2$ are less than 300 m/s (electric fields less than ~15 mV/m). This means conditions are below the ion-acoustic speed threshold for excitation of the two stream, or Farley-Buneman, instability (e.g., see Fejer and Kelley, 1980). In this plot, the bottomside distribution of positive scale lengths becomes narrower, with the sharpest gradients overwhelmingly dominating below about 98 km. Low electric fields mean either there is no magnetic activity or there is strong activity but EISCAT observes inside regions of very energetic precipitation (auroral arcs) where N_e increases sharply and peaks at lower altitudes, while the electric field drops because of conductivity enhancements. In the present analysis no attempt was made to differentiate between the two possible cases.

The middle panel in Fig. 6 illustrates the situation for moderate electric fields between 15 and 40 mV/m (V_d is between about 300 and 800 m/s). This represents a typical auroral situation during which the plasma is unstable with regard to the two stream instability and Type 1 echoes are detected routinely by VHF radars like STARE (Haldoupis 1989). Compared to the situation depicted in the top panel, in this instance the bottomside distribution becomes broader and expands in altitude so that the occurrence of small gradient scale lengths are equally probable over an altitude range between about 95 and 105 km.

Finally, the gradient scale length distribution was found to be quite different during times of very intense electric fields, as illustrated in the bottom panel of Fig. 6. There, only N_e profiles for electric fields larger than 40 mV/m are considered. As seen, the distribution has a single peak now at a higher altitude near 108 km, in sharp contrast to the situation prevailing during low electric fields when the dominant gradients are located near 96 km. This is in line with the observation that during times of strongly elevated electric fields, electron densities decrease drastically at altitudes lower than about 105 km and the N_e profile moves up in altitude, peaking near 110 km (St.-Maurice *et al.*, 1990).

Finally, an effort was made in our analysis to determine if the measured vertical density gradients exhibit any systematic difference for the eastward and westward auroral electrojets. The nature of these two Hall current systems, which dominate the pre-midnight and post-midnight time sectors respectively, can be different. In general, the eastjet is well defined in height and altitude and remains fairly steady in direction, contrary to the westjet which is much more variable and dynamic (e.g., see Kamide and Brekke, 1977; Araki *et al.*, 1989; Haldoupis *et al.*, 1990). This is because the eastjet is closely related to diffuse aurora caused by a relatively steady flux of low energy particles, whereas the westjet associates with energetic and dynamic particle precipitation with energies of at least several keV. As a consequence, the electron density profiles in the *E*-region can be different in the eastjet and westjet, and one would therefore expect some differences to exist in the vertical density gradients resulting from these profiles.

As seen from Fig. 3, the CP1 data used in the analysis are equally representative of both electrojet systems. By using the measured electron drift (or electric field) direction, two sets of electron density profiles were formed, each representing the eastward and westward electrojet. Then, the same methodology was applied to determine the distributions of the vertical gradient scale lengths as a function of altitude for different electric field levels. The results are summarized in the form of occurrence distributions in the color-coded plots of Fig. 7 for low ($E < 15$ mV/m), moderate, and high ($E > 40$ mV/m) electric fields.

An overall inspection of Fig. 7 shows that, on average, there are no great differences in the distributions

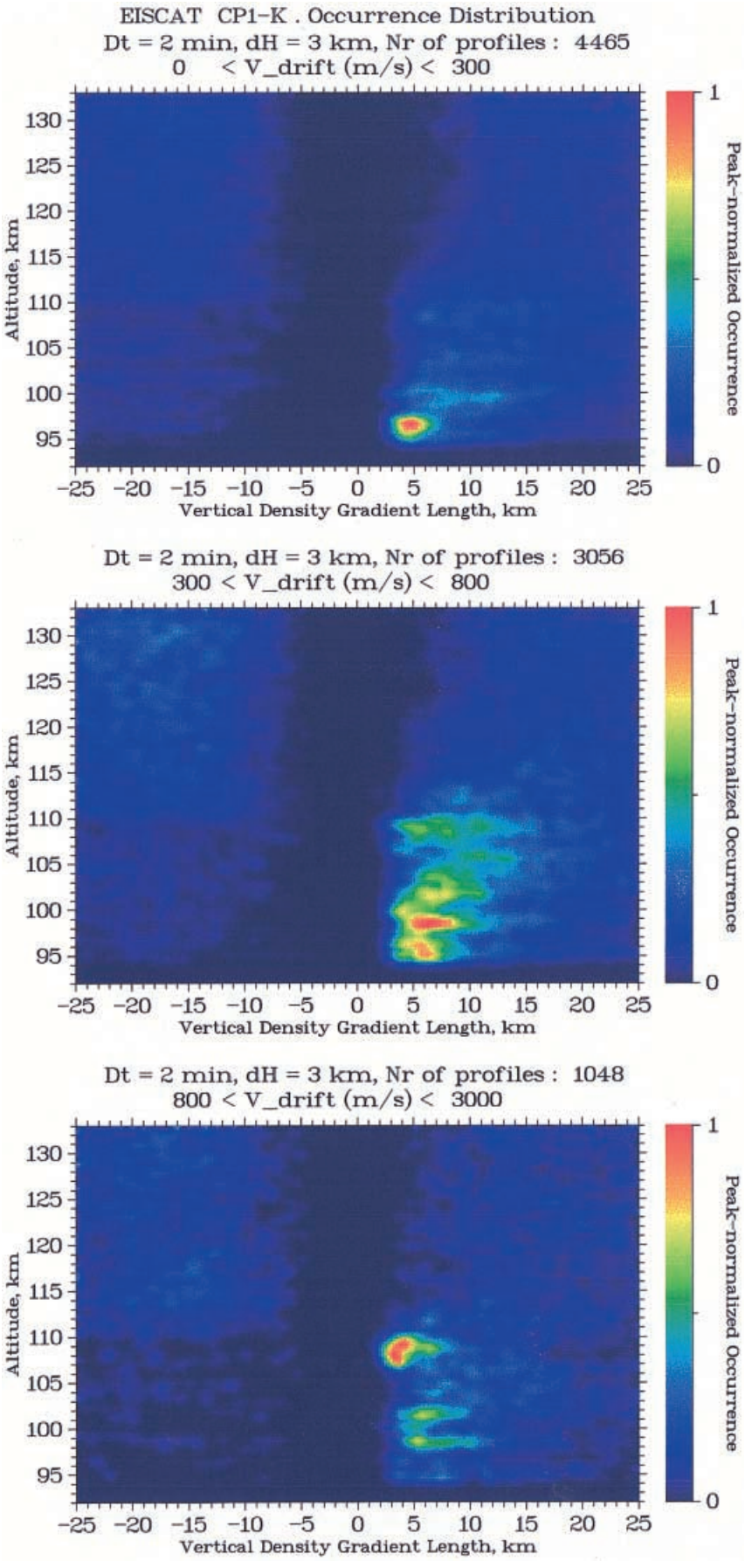

Fig. 6. Same as Fig. 5 but now the distributions correspond to three different electron drift (or electric field) ranges. The *upper one* is for low electric fields (less than 15 mV/m), the *middle one* is for moderate fields, and the *bottom one* for large fields (larger than 40 mV/m)

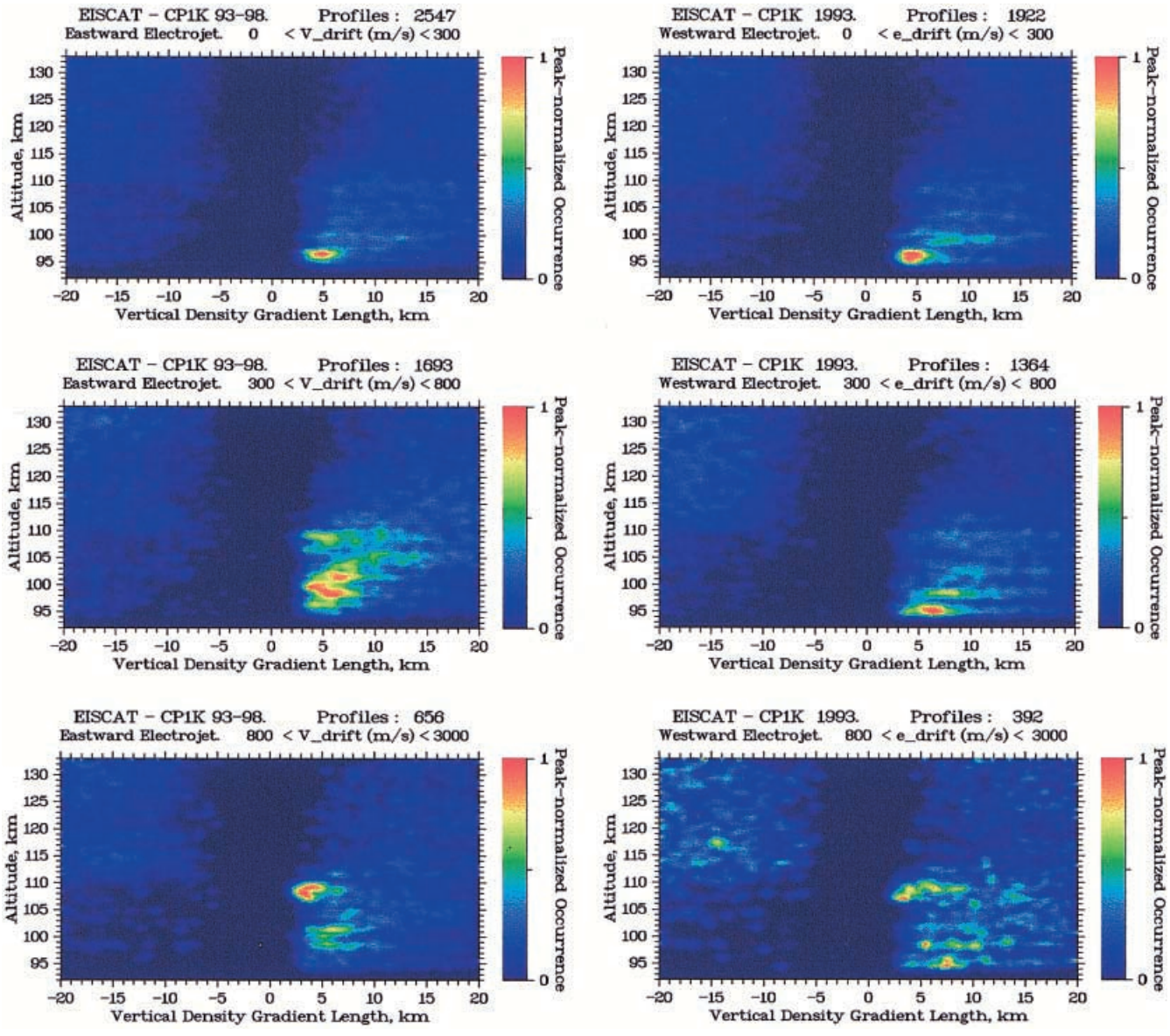

Fig. 7. Same as Fig. 6, but now the data are separated to represent those corresponding to eastward electrojet (*left panels*) and westward electrojet (*right panels*)

of occurrence with altitude for the eastward and westward electrojet. This is particularly true during low electric field conditions. As seen in the leftmost panels where electron drifts are fairly low ($V_d < 300$ m/s), the corresponding distributions for the eastjet and westjet are, for all practical purposes, the same. As we move to higher electron drifts, however, some differences do exist which seem to be significant. In the middle plots, for example, we see that the eastjet distribution peaks on the average at higher altitudes than its westjet counterpart. Apparently, this reflects the difference which is known to exist in altitude between eastjet and westjet (e.g., Kamide and Brekke, 1977) resulting from the difference in the energy of precipitating particles, and possibly by vertical plasma motions caused by the large electric fields in accordance with a model presented by Huuskonen *et al.*, (1984). Also, the eastjet distribution is narrower and statistically more stable than that of the westjet. As for strongly elevated electric fields, the westjet distribution (rightmost bottom panel) is more structured compared to the eastjet one (rightmost top panel). Most likely, these differences reflect the variable and dynamic nature of the westward electrojet.

5 Theoretical implications

Next, the objective is to assess, at least approximately, the importance of the present findings relative to the auroral *E*-region plasma instability process. As discussed, the gradient drift term in the dispersion relation relates to the density gradient component perpendicular to the magnetic field, and therefore the scale length of importance is not L_z, but rather $L_\perp = L_z/\cos I$. In this

way, the measured vertical density gradients must be scaled according to magnetic dip at a given location. Considering for example $L_z = 5$ km, the corresponding $L_\perp$ will range between about 15 and 30 km for auroral zone magnetic dip angles between about 70° and 80°. For a magnetic dip angle of 76.5°, that is close to the the EISCAT site, the shortest and most probable scale lengths perpendicular to the magnetic field, $L_\perp$, are confined to the bottomside of the *E*-region peak, that is, below 110 km, and point northward taking values between about 10 and 50 km. On the other hand, at the topside the most probable scale lengths $L_\perp$ are longer than 40 to 50 km and point southward. Obviously, the bottomside gradients are much more effective in the instability process than the topside ones.

The destabilizing and stabilizing effects of a density gradient have been studied extensively in the literature (e.g., see Farley and Fejer, 1975; Fejer *et al.*, 1984, among many others). Next, an effort will be made to highlight the implications of our findings by considering some indicative numerical calculations and approximate estimates. Following Fejer *et al.* (1984), the phase velocity of marginally stable waves, that s, if $\gamma_k = 0$ in Eq. (2), takes the form

$$V_{th} = C_s[(F^2 + G + 1)^{1/2} - F] \ , \qquad (4)$$

where

$$F = \frac{\nu_i \Omega_e}{2\nu_e k^2 L_\perp C_s}, \qquad G = \frac{2\alpha N_e \nu_i (1 + \Psi)}{k^2 C_s^2 \Psi} \ .$$

F and G are terms representing the electron density gradient and recombination contributions, respectively. To obtain representative estimates, we consider a lower rather than a higher altitude, because the sharpest gradients are observed at lower *E*-region altitudes during low to moderate electric fields, that is, when the role of a density gradient in the instability process becomes most important.

Indicative numerical results are presented in Fig. 8, which shows the required electron drift velocity V_d, or the normalized drift velocity V_d/C_s, at instability threshold as a function of irregularity wavelength for both stabilizing (solid lines) and destabilizing (dashed lines) scale lengths $L_\perp$. The gradient lengths of 10 and 50 km were chosen to be in accordance with our measurements and represent range limits for the most probable perpendicular gradients expected to occur at the bottomside of the auroral zone *E*-region. It is important to stress that $L_\perp$ associates with $(\nabla N_e)_z$, which lies in the magnetic meridian plane (Greenwald, 1974). The curves in Fig. 8 were obtained from Eq. (4) at 100 km, where nominal values for the plasma parameters are as follows: $C_s = 325$ ms^{-1} (assuming isothermal ions and electrons and no significant electron gas heating), $\nu_i = 4.6 \times 10^3$ s^{-1}, $\nu_e = 4.7 \times 10^4$ s^{-1}, $\Omega_i = 180$ s^{-1}, $\Omega_e = 10^7$ s^{-1}, and $2\alpha N_e = 0.06$ s^{-1} in line also with Fejer *et al.* (1984). As expected, the destabilizing effects of a density gradient on the instability threshold are much more severe at longer wavelengths λ, provided that $\lambda \ll L_\perp$. On the other hand, the stabilizing action of the gradients can be quite severe even if λ is as short as 10 to 20 m.

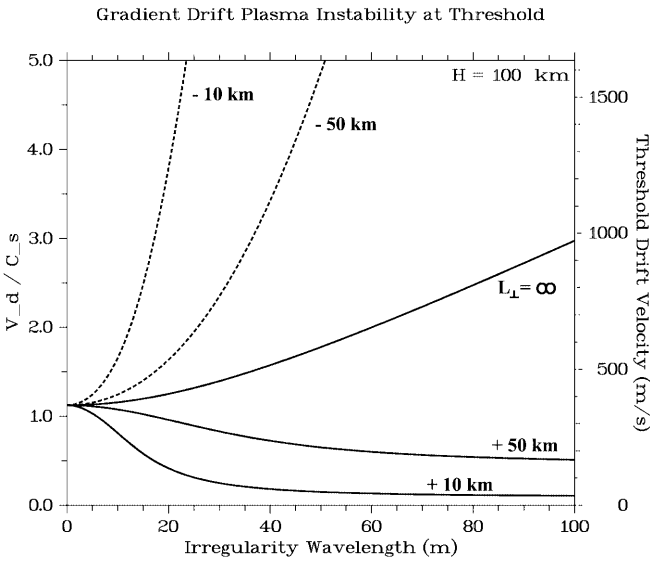

Fig. 8. Gradient drift instability threshold predictions at 100 km for irregularity wavelengths up to 100 m. The *curves* correspond to the most probable scale lengths, ranging between 10 and 50 km, as measured by EISCAT in the bottomside *E*-region. The destabilizing gradients (*solid curves*) relate to eastward electrojet, whereas the stabilizing gradients (*dashed curves*) refer to the westward electrojet conditions. The *curve labeled* $L_\perp = \infty$ represents the instability threshold in the absence of any gradient in electron density. This figure is similar to Fig. 2 of Fejer *et al.* (1984)

Since Fig. 8 applies to the the *E*-region bottomside, the destabilizing (solid-line) curves refer to the eastward electrojet when the electric field is northward, that is, it points in the same direction as $(\nabla N_e)_\perp$ (e.g., see geometry in Fig. 1). On the other hand, the stabilizing (dashed-line) curves apply for the westward electrojet when the electric field points southward, therefore being opposite to $(\nabla N_e)_\perp$. Of course the situation we describe here would reverse if we took the ambient vertical gradients at the *E*-region topside. Although we show no representative numerical results, the topside gradient effects, especially the destabilizing ones, are much less important than those at the bottomside, as discussed also by Fejer *et al.* (1984). This is not only because the measured topside gradients are less steep and less likely to occur, but also because the instability threshold is higher due to higher temperatures and, in addition, the relative electron-ion drift velocities are steadily reduced with altitude because the ions tend to $\mathbf{E} \times \mathbf{B}$ drift as well.

In view of this discussion, the main implication of our findings relates to the steep bottomside vertical gradients and their anticipated impact for the unstable state of plasma in the eastjet and westjet. In relation to Fig. 1, Fig. 8 suggests that the auroral *E*-region bottomside must be strongly unstable to long wavelength waves of several tens to hundreds of meters generated directly by the gradient drift instability and propagating westward along $\mathbf{E} \times \mathbf{B}$. On the other hand, and in sharp contrast to the eastjet, the westward electrojet plasma at the bottomside should be strongly stable to the gradient drift instability for wavelengths higher than a few

meters. Some evidence in favor of these implications was reported by Pfaff *et al.* (1984) from in situ observations made with a low-apogee auroral rocket flight inside an eastward electrojet. They observed large wavelength electrostatic fluctuations on the bottomside where the vertical density gradient was upward. These were polarized along the $\mathbf{E} \times \mathbf{B}$ direction and found to be reduced in amplitude above about 107 km when the vertical gradient in electron density changed direction.

Finally, we make a brief reference to HF and VHF auroral radar backscatter caused by decameter and meter scale plasma waves, respectively. Figure 9, which is the same as Fig. 8 but focuses on wavelengths up to 20 m, shows the effect of the measured bottomside gradients to be rather small for direct generation of meter-scale waves which are observed by VHF radars ($\lambda < 5$ m). On the other hand, these gradients could have a significant effect in lowering the instability threshold for 10 to 20 m wavelength irregularities in the bottomside of the eastward electrojet. In particular, this would be of importance in the direct generation of decameter irregularities in the eastjet bottomside when electric fields are lower than 10 to 15 mV/m, that is, when the two stream instability mechanism is inoperable. These decameter primary waves will propagate mostly westward and, in principle, can be detected if an HF radar beams at large azimuths along the Hall current direction. On the other hand, one should expect to observe at small azimuths, shorter-scale, secondary waves generated indirectly from the large-scale decameter gradient drift primaries through non-linear wave interaction and energy cascade (Sudan, 1983).

Provided that our basic theoretical understanding is valid, our observations imply that, particularly during low electric fields, an auroral radar should be capable of receiving plenty of echoes from the *E*-region bottomside in the eastjet time sector but no scatter in the westjet sector because there the plasma must be strongly stable to the gradient drift instability. We suggest these implications can be tested in a carefully run auroral Doppler radar experiment, particularly with the deployment of a vertical radar interferometer.

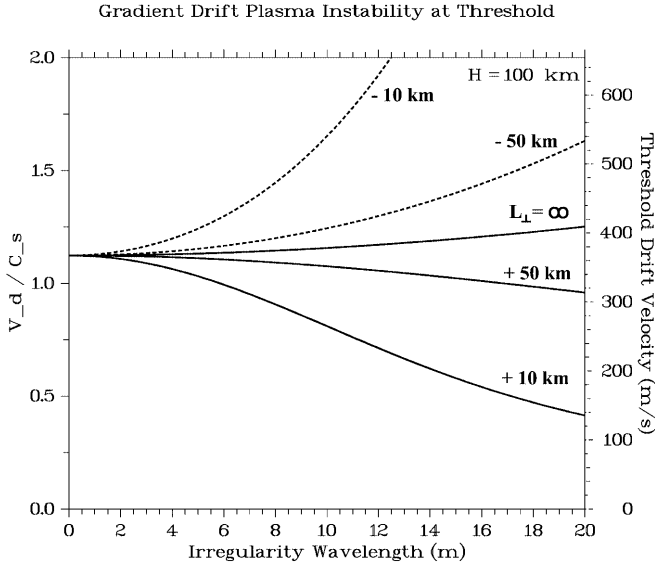

Fig. 9. Same as Fig. 8, but only for irregularity wavelengths up to 20 m, that is, for irregularity scales which may be detectable by HF-VHF auroral backscatter radars

6 Summary

EISCAT CP1 data were used to study statistically the ambient vertical density gradients in auroral *E*-region altitudes. Our findings are summarized as follows:

1. The prevailing vertical electron density gradients, $(\nabla N_e)_z$, are positive, having characteristic gradient lengths $L_z = N_e/(\nabla N_e)_z$ ranging between 4 to 7 km. At low electric fields they are located at the bottomside of the *E*-region peak near 95 km, but move progressively up in altitude during conditions of increased electric fields.
2. The sharpest $(\nabla N_e)_z$, with L_z possibly less than 3 km, are observed near 108 km mostly in the eastward electrojet during times of elevated electric fields, that is, fields greater than 40 to 50 mV/m.
3. Negative $(\nabla N_e)_z$ prevail above about 112 km, but are much weaker than the positive ones, with L_z between 10 and more than 25 km.
4. On average, there are no major differences in the observed vertical electron density gradients in the eastward and westward electrojets. The few differences observed associate mostly with large electric field conditions and reflect the different nature of the currents with relation to diffuse and discrete auroras.

Also, the linear gradient drift instability was applied to assess the implications of our findings. These are as follows:

1. The vertical gradients $(\nabla N_e)_z$ can strongly destabilize the plasma at long wavelengths (tens to hundreds of meters) in the bottomside *E*-region during times of low electric fields, but only in the eastward electrojet.
2. The bottomside gradients are expected to be strongly stabilizing in the westjet when the electric field is southward. This suggests that the unstable state of the low *E*-region auroral plasma may be drastically different for the eastward and westward electrojets.
3. The generated long wavelength irregularities propagate mainly along the east-west direction and may be capable of generating shorter scale secondary waves in other directions.
4. The bottomside gradients can directly generate decameter-scale waves, which could be observed by HF radars beaming at large azimuths, but not meter-scale waves (seen by VHF radars).
5. The topside *E*-region density gradients are fairly weak and therefore contribute less to the unstable/stable state of the plasma.

Acknowledgements. One author (C.H.) thanks Max-Planck-Gesellschaft for providing support for a two month visit at Max-Planck Institut für Aeronomie during summer 1999, when a large part of this work was completed. The European Incoherent Scatter

radars (EISCAT), are supported by the national scientific agencies of Finland, France, Germany, Norway, Sweden, United Kingdom and Japan.

Topical Editor M. Lester thanks T. Bösinger and S.E. Milan for their help in evaluating this paper.

References

Araki, T., K. Schlegel, and H. Lühr, Geomagnetic effects of the Hall and Pedersen current flowing in the auroral ionosphere, *J. Geophys. Res.*, **94,** 17 185, 1989.

Bourdillon, A., C. Haldoupis, and J. Delloue, High-frequency Doppler radar observations of magnetic aspect sensitive irregularities in the midlatitude *E* region ionosphere, *J. Geophys. Res.*, **100,** 21 503, 1995.

Farley, D. T., and B. G. Fejer, The effect of the gradient drift term on the type 1 electrojet irregularities, *J. Geophys. Res.*, **80,** 3087, 1975.

Fejer, B. G., and M. C. Kelley, Ionospheric irregularities, *Rev. Geophys. Space Phys.*, **18,** 401, 1980.

Fejer, B. G., D. T. Farley, B.B. Balsley, and R. F. Woodman, Vertical structure of the VHF backscattering region in the equatorial electrojet and the gradient drift instability, *J. Geophys. Res.*, **80,** 1313, 1975.

Fejer, B. G., E. Providakes, and D. T. Farley, Theory of plasma waves in the auroral *E*-region, *J. Geophys. Res.*, **89,** 7487, 1984.

Greenwald, R. A., Diffuse radar aurora and the gradient drift instability, *J. Geophys. Res.*, **79,** 4807, 1974.

Haldoupis, C., A review on radio studies of auroral *E*-region ionospheric irregularities, *Ann. Geophysicae*, **7,** 239, 1989.

Haldoupis, C., and K. Schlegel, A 50 MHz radio Doppler experiment for midlatitude *E* region coherent backscatter studies: system description and first results, *Radio Sci.*, **28,** 959, 1993.

Haldoupis, C., K. Schlegel, and E. Nielsen, Dependence of radar auroral scattering cross section on the ambient electron density and the destabilizing electric field, *Ann. Geophysicae*, **8,** 195, 1990.

Haldoupis, C., G. J. Sofko, G. C. Hussey, and J. Mu, An overview of type-3 radar auroral research: basic observational properties and new interpretation propositions, *Ann. Geophysicae*, **13,** 10, 1995.

Huuskonen A., T. Nygren, L. Jalonen, and J. Oksman, The effect of electric field-induced vertical convection on the precipitation *E*-layer, *J. Atmos. Terr. Phys.*, **46,** 927, 1984.

Kamide, Y. R., and A. Brekke, Altitude of the eastward and westward auroral electrojets, *J. Geophys. Res.*, **82,** 2851, 1977.

Kelley, M.C., *The Earth's ionosphere: plasma physics and electrodynamics*, Academic, San Diego, California, 1989.

Pfaff, R. F., Rocket studies of plasma turbulence in the equatorial and auroral electrojets, *PhD Thesis*, Cornell University, Ithaca, N. Y., 1986.

Pfaff, R. F., M. C. Kelley, B. G. Fejer, E. Kudeki, C. W. Carlson, A. Pedersen, and B. Hausler, Electric field and plasma density measurements in the auroral electrojet, *J. Geophys. Res.*, **89,** 236, 1984.

Pfaff, R. F., M. C. Kelley, E. Kudeki, B. G. Fejer, and K. D. Baker, Electric field and plasma density measurements in the strongly driven daytime equatorial electrojet, *J. Geophys. Res.*, **92,** 13 597, 1987.

Riggin, D., W. E. Swartz, J. F. Providakes, and D. T. Farley, Radar studies of long wavelength waves associated with mid-latitude sporadic E layers, *J. Geophys. Res.*, **91,** 8011, 1986.

Schlegel, K., Auroral zone *E*-region conductivities during solar minimum derived from EISCAT data, *Ann. Geophysicae*, **6,** 129, 1988.

Schlegel, K., and J.-P. St.-Maurice, Anomalous heating of the polar *E* region by unstable plasma waves. 1. Observations, *J. Geophys. Res.*, **86,** 1447, 1981.

St.-Maurice, J.-P., W. Kofman, and E. Kluzek, Electon heating by plasma waves in the high latitude *E*-region and related effects, *Adv. Space Res.*, **10**(6), 225, 1990.

St.-Maurice, J.-P., P. Prikryl, D. W. Danskin, A. M. Hamza, G. J. Sofko, J. A. Koehler, A. Kustov, and J. Chen, On the origin of narrow non-ion acoustic radar spectra in the high-latitude *E* region, *J. Geophys. Res.*, **99,** 6447, 1994.

Sudan, R. N., Unified theory of type I and type II irregularities in the equatorial electrojet, *J. Geophys. Res.*, **88,** 4853, 1983.